Modeling anomalous electron transport in Hall thrusters

By E. Fernandez †, M. Cappelli ‡ N. Gascon ‡ AND M. Allis ‡

We examine the issue of electron mobility in Hall thruster plasmas using two hybrid models, one in the radial and axial coordinates ($r - z$ model), and the other in the azimuthal and axial coordinates ($z - \theta$ model). Unlike most $r - z$ simulation efforts, which model the electron transport via an *ad hoc* Bohm parameter, the $r - z$ model presented here uses a transport parameter based on a recent experimental measurement (Meezan, Hargus & Cappelli 2001). An examination of equilibrium profiles as well as $I - V$ curves reveal marked improvement over the simpler Bohm scaling results. Motivated by these results and the need to incorporate azimuthal effects, we formulate a new $z - \theta$ model. It is presented here as the simplest description of Hall thruster plasmas able to capture the azimuthal drifts absent in $r - z$ formulations. Preliminary results show that transport arising from azimuthal disturbances can be significant.

1. Introduction

1.1. *Motivation and objectives*

Hall thrusters represent an electric propulsion technology that has attracted considerable interest concomitant with the increased number of government and commercial satellites in orbit (Gulczinski & Spores 1996). The main use of these small, high specific impulse rockets lies in low thrust applications like orbit transfer and orbit station keeping. In Hall thruster plasmas, electrons emanating from a cathode ionize xenon neutrals upon collision. The resulting ions are accelerated out of the device by the electric potential drop between the cathode and the anode, typically a few hundred volts. Such potential drop is localized near the exit of the device by an external radial magnetic field set up by an electromagnet. While the overall operation of these thrusters is understood, key physics issues remain open for investigation. Of particular interest is the study of electron transport in these engines. It is well known that the electron conductivity in the Hall thruster is much larger than can be inferred from classical collisions alone (Morozov, Esinchuk, Tilinin, Trofimov, Sharov & Shchepkin 1972). Turbulent fluctuations and wall effects are believed to have a major effect on the enhanced conductivity, which, in turn, affects the electric field, ionization, thrust, and overall discharge behavior. A good understanding of the processes involved in determining this anomalous transport remains the subject of important research, not only in regard to Hall thruster plasmas but fusion and astrophysical plasmas as well.

With the exception of the works by Hirakawa (Hirakawa & Arakawa 1996) and Adams (Adams, Heron & Laval 2004), prior computational work on Hall thrusters has been in one dimension (1D) in the axial direction or two dimensions (2D) in the axial and radial directions. These works have had reasonable success in describing the overall behavior of

† Eckerd College
‡ Mechanical Engineering Department, Stanford University

the plasma discharge. Most notably, they have recovered the dominant instability in these devices - the so-called "breathing mode" instability. However, a key element is missing in these descriptions: azimuthal dynamics. Besides drifting axially opposite to the electric field, electrons in the thruster drift azimuthally as a result of the imposed electric and magnetic fields. Azimuthal perturbations arise from the established equilibrium and, if properly correlated, result in a net axial transport of electrons (Janes & Lowder 1966). This effect is not captured in $r - z$ descriptions and needs to be modeled.

Most 2D works have used a Bohm mobility given by

$$\mu = \frac{1}{16B} \qquad (1.1)$$

as a model for the enhanced conductivity (Fernandez, Cappelli & Mahesh 1998). Recently, some works have used a Bohm scaling for the mobility with a constant other than $\frac{1}{16}$ in order to better fit experiments (Bareilles, Hagelaar, Garrigues, Boniface, Boeuf & Gascon 2004). Nonetheless, many plasma transport experiments (outside of Hall thrusters) have demonstrated that electron transport can vary greatly and does not always conform to a Bohm scaling. More importantly, a recent, first direct measurement of electron mobility in Hall thrusters has revealed that such transport is a complicated function of axial location as well as operating parameters (Meezan, Hargus & Cappelli 2001). In particular, at high voltage, Bohm transport seems to fare well in the middle of the channel while at the channel exit the transport is reduced to near its classical value. The experiment, in fact, suggests that a single model does not properly describe the full plasma region from the anode to the near plume. With this experimental observation as our main motivation, our objectives for this paper are a) modify the $r - z$ model by incorporating an *experimentally-based* mobility, and b) construct a $z - \theta$ model which self-consistently evolves the azimuthal drifts and makes no use of transport parameters.

This rest of this paper is organized as follows. Section II describes the $r - z$ model and compares results using Bohm mobility and experimentally based mobility. Section III describes the $z - \theta$ model and the preliminary results from such simulations. Finally, section IV concludes the paper with the conclusions and future work.

2. $r - z$ **model**

2.1. *Overview*

A detailed description of the $r - z$ model is given elsewhere (Allis, Gascon, Vialard-Goudou, Cappelli & Fernandez 2004). Here we just present a summary. The radial and axial description of the Hall thruster plasma is based on the model by Fife at MIT (Fife 1995). Electrons, single-ionized xenon ions and xenon neutrals are time-advanced in a geometry that extends from the anode to the inner plume. We assume no azimuthal variation in the plasma quantities; the simulation effectively represents a slab of plasma in the radial and axial directions at an arbitrary azimuthal angle. The model assumes a constant external magnetic field (produced by the electromagnet) and neglects the much smaller magnetic field created by the plasma.

The heavy particle species - ions and neutrals - are fairly collisionless and are described via the particle-in-cell (PIC) method. Neutral superparticles are injected into the domain at the anode position at a prescribed rate. They are, in turn, ionized by electron-impact ionization collisions. The ions born in the ionization process, due to their large inertia, are effectively unmagnetized and respond only to the electric field. Upon colliding with the thruster walls, ions recombine to form neutrals which are then injected into the domain.

The neutrals, not being affected by electromagnetic forces, only modify their velocities if they collide with the walls of the thruster. Elastic collisions among ions and neutrals are assumed small and thus neglected (however, some effects like charge-exchange have recently been considered (Allis, Gascon, Vialard-Goudou, Cappelli & Fernandez 2004)).

The electrons, unlike the heavy xenon ions, are strongly magnetized and are treated as a fluid. The fluid equations that are used are current conservation, parallel and perpendicular (with respect to the magnetic field) momentum, and electron energy. The system is closed by specifying the electric field and imposing quasineutrality. The set of equations is given by:

$$I_a = \int_A (n_i u_{i\hat{n}} - n_e u_{e\hat{n}}) dS \tag{2.1}$$

$$\phi = \frac{kT_e}{e} \ln n_e + \phi^* \tag{2.2}$$

$$\mathbf{E} = -\nabla \phi \tag{2.3}$$

$$u_{e\hat{n}} = -\mu \left(E_{\hat{n}} + \frac{kT_e}{en_e} \frac{\partial n_e}{\partial \hat{n}} + \frac{k}{e} \frac{\partial T_e}{\partial \hat{n}} \right) \tag{2.4}$$

$$\frac{\partial}{\partial t} \left(\frac{3}{2} n_e kT_e \right) + \frac{\partial}{\partial \hat{n}} \left(\frac{5}{2} n_e u_{e\hat{n}} kT_e - K \frac{\partial T_e}{\partial \hat{n}} \right) = -\dot{n}_e \varphi(T_e) E_i - \alpha T_e^{3/2} + j_{e\hat{n}} E_{\hat{n}} \tag{2.5}$$

$$n_i = n_e \tag{2.6}$$

where the $\hat{n}$ symbol means perpendicular to the magnetic field. The symbols I_a, n_i, n_e, $u_{i\hat{n}}$, $u_{e\hat{n}}$, ϕ, k, T_e, e, ϕ^*, $\mathbf{E}$, μ, K, $\dot{n}_e$, $\varphi(T_e)$, E_i, α, $j_{e\hat{n}}$, stand for the discharge current, ion density, electron density, ion velocity, electron velocity, electrostatic potential, Boltzmann constant, electron temperature, electron charge, magnetic field contour constant, electric field, electron mobility, thermal diffusivity, ionization rate, ion production cost, ionization potential, wall loss coefficient and electron current density respectively.

The current conservation equation (eqn. 2.1) says that the total (ion plus electron) electric current cutting each magnetic field contour is constant and equal to the discharge current collected at the anode. It also assumes that no current is lost parallel to the magnetic field. Equation 2.2 is known as Boltzmann relation, and it follows from a balance of electric and pressure forces. The field equation (eqn. 2.3) says that the electric field is purely electrostatic, as magnetic perturbations are small and neglected. The perpendicular momentum equation (eqn. 2.4) is set by electric, pressure and collisional drag forces. However, inertial terms as well as important azimuthal drifts have been neglected. These, and presumably other effects like wall-induced conductivity, are *effectively* captured by using an enhanced mobility μ. The mobility can be given by its Bohm value (eqn. 1.1), or, as seen later, by an experimentally motivated form. In the electron energy equation (eqn. 2.5), the three terms on the right hand side represent ionization losses, wall losses, and joule heating respectively (Fife 1995). We note that the wall-loss term in the temperature equation assumes a constant secondary electron emission coefficient equal to .6 in the present model (Lentz 1990). A more realistic wall-loss term, which takes into account the temperature dependence of the secondary electron emission coefficient as well as sheath saturation effects, will be the subject of future work.
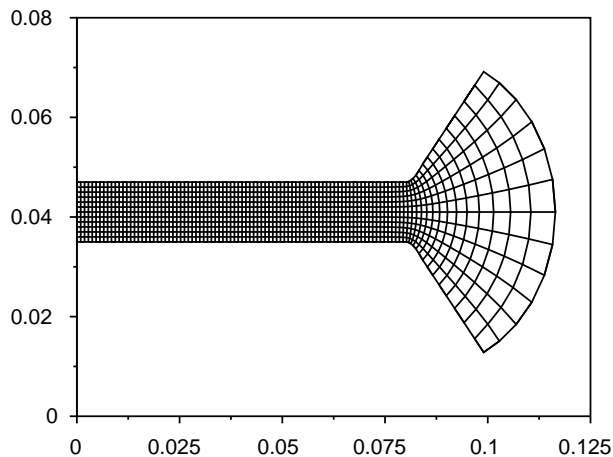
FIGURE 1. Grid for Stanford Hall thruster. The vertical and horizontal axes represent the radial and axial distance respectively. Both distances are in meters.

2.2. *Numerical method*

2.2.1. *Geometry, grid and magnetic field*

Stationary Plasma Thruster (SPT 100) and Stanford Hall Thruster (SHT) geometries are considered, but the results presented here use the SHT geometry. Given the geometry, a nonuniform orthogonal grid of 101 by 13 grid points in the axial and radial directions is constructed. The grid, covering the full channel region and inner plume is shown in Figure 1. Once the grid is obtained, the constant external magnetic field is computed using Laplace's equation. Alternatively, the full 2D the magnetic field profile can be obtained from experimental data. The peak of the external magnetic field is on the order of a hundred gauss, mostly in the radial direction, and located just inside the channel exit.

2.2.2. *PIC method*

The heavy species are described with a PIC method. The standard leap-frog scheme is used to advance the positions and velocities of the particles. Their densities are then obtained at each grid point via bilinear interpolation. Since the time scale of these particles is much slower than that of the electrons, both ions and neutrals are advanced every so many electron-fluid time steps. As is typical of PIC codes, the particles themselves are superparticles, representing a conglomeration of unit particles. In addition, in this code the superparticles are of variable mass. This allows for the efficient handling of regions in the channel with high density and regions with very low density. The ionization of neutrals is done with a Monte Carlo technique. By allowing the ion superparticles to have variable mass, one can dictate the number of ions born in a given cell per timestep, and avoid having cells with too many or too few superparticles. The number of superparticles in the simulation eventually reaches an equilibrium, where the number of neutrals leaving the domain at the downstream boundary, plus those lost through ionization, balance the number of neutrals injected at the anode and those born through ion-recombination at the channel walls. Similarly, the ions lost by wall collisions and those lost by leaving the downstream boundary are balanced by the ions born through ionization events. However,

this equilibrium is not steady and strong oscillations take place (Fernandez, Cappelli & Mahesh 1998). The PIC method couples to the electron fluid method through quasineutrality: the electron density is obtained from the ion density.

2.2.3. *Fluid method*

Owing to the large parallel electron thermal conductivity, the electron temperature in the thruster can be considered constant along each magnetic contour. Thus, the temperature is solved for each contour λ rather than for each grid point. Specifically, this is done by substituting equations 2.2-2.4 into 2.5, and projecting along λ. The equation that follows is then discretized using a finite difference scheme for the spatial terms, and the resulting system of equations is solved with a fourth-order Runge-Kutta scheme. Two hundred λ contours are used in order to resolve the sharp gradients near the channel exit. The boundary conditions for the temperature are Neumann for the first contour and Dirichlet for the last contour (the first contour is that which just touches the anode and the last contour is that which just touches the cathode). Having obtained the temperature, the electric potential is obtained. Then the algorithm checks if the resulting anode potential is close to the prescribed boundary condition anode potential. If it is, then algorithm proceeds to the next time step. If the potential boundary condition is not met, then a Newton's method on the discharge current I_a is used until the condition is satisfied. The electron fluid algorithm thus solves for the electron temperature, discharge current and electric potential. The field equation (eqn. 2.3) then gives the electric field which is used to advance the particles, and the whole process is repeated until an equilibrium in plasma quantities is established.

2.3. *Results*

It is important to mention that our objective in this section is to investigate the *qualitative* effect of using various mobility models on simulation results. A more thorough examination that looks at charge-exchange collisions, specular versus diffuse wall scattering, reverse ion flow, inflow of background neutrals, and refined inputs for the ionization rate and experimental mobility, has been done by Allis (Allis, Gascon, Vialard-Goudou, Cappelli & Fernandez 2004). Similarly, $r-z$ model studies that look at breathing-mode and transit-time oscillations are taken up elsewhere (Gascon, Allis, Thomas, Cappelli & Fernandez 2004).

Experimental data indicates that the transport in the SHT is Bohm-like except near the anode and channel exit (Meezan, Hargus & Cappelli 2001). In the latter region, the mobility decreases and comes up again within two centimeters (goes through a dip). At its minimum value, the mobility approaches the "classical value". Interestingly, this region of transport surpression corresponds to a highly sheared electron flow region, and is reminicent of fusion plasmas where transport has been successfully lowered to classical levels by inducing a sheared flow. Whether the shear surpression mechanism of fusion plasmas is indeed responsible for the dip in the Hall thruster mobility is an open question. Regardless of the mechanism, we can construct an experimentally-motivated expression for the mobility for use in simulations as follows:

$$\mu = \frac{1}{\alpha + \beta \left(\frac{\sin 300(z-.077)}{300(z-.077)} \right)^2} \frac{1}{B} \tag{2.7}$$

where α and β and are parameters representing the base line transport level and depth of the dip respectively. The value of .077 corresponds to the location of the dip, which is

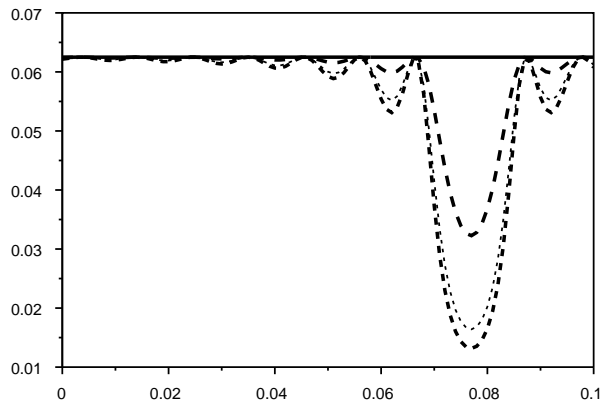*E. Fernandez, M. Cappelli, N. Gascon & M. Allis*

FIGURE 2. Experimentally based mobility model. The vertical axis is dimensionless. The horizontal axis represents axial distance (the channel exit corresponds to .08). The solid trace corresponds to Bohm transport. The bold dotted trace, the dotted trace and the bold dashed trace correspond to the experimentally based mobility for 200, 160 and 120 volts respectively.

centered around the peak of the magnetic field. The factor of 300 in the formula above is used to confine the dip to about 2cm in width. Simple Bohm transport corresponds to $\alpha = 16$ and $\beta = 0$. Experiment shows that the dip gets deeper as the voltage increases, and β is chosen to reflect this trend. Figure 2 shows the mobility for various values of β. We point out that the transport reflected by equation 2.7 goes into the expression we use for the thermal conductivity in the energy equation (eqn. 2.5). Thus, the mobility model affects not only the momentum equation, but also the energy equation through convection *and* thermal conduction effects. Finally, we note that the actual form of equation 2.7 is not what is important here – all we are after is an expression that captures the trends in the experimental data.

In order to assess the effect of the transport coefficient μ on the simulation we present, in Figure 3, $I - V$ curves from three sets of simulations at flow rates of 3mg/s, and experimental data at 2mg/s. In comparing the experimental and simulation $I - V$ curves one should increase the experimental curve values by about 50% to compensate for the two different mass flow rates. It is clear that the experimentally-based mobility does better than the Bohm mobility. The most significant disagreement takes place at low voltage: in the experiment the current drops to zero at about 60 volts whereas in the simulation this happens at 90 volts. In addition, the simulation does not recover the inflection point at about 120 volts - a robust feature in these discharges that lacks explanation at the present time.

More striking is the effect of the mobility on equilibrium profiles, as shown in Figures 4 and 5 (bold, dotted and solid traces represent the experimental, Bohm simulation, and experimentally-based simulation profiles respectively in each figure). Figure 4 shows the electron temperature peaking outside the channel for the Bohm mobility case, something not seen experimentally. In addition, the sharp gradient near the channel exit is not realized. The simulation using the experimentally based mobility clearly does better. It is interesting to note the high temperature near the anode in the experimental curve – something which is seen only at high voltage. Neither model recovers this; a closer examination of this region is the subject of future work. In Figure 5, most of the electric
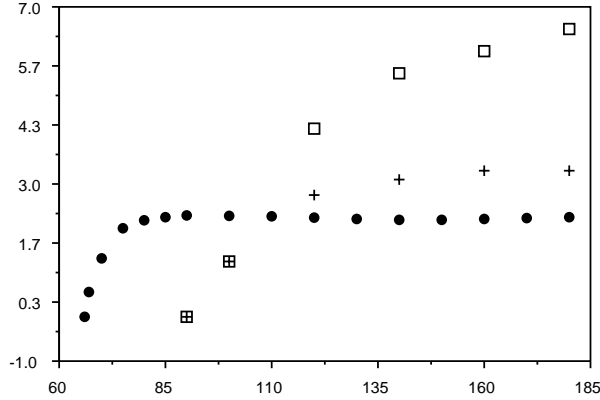
FIGURE 3. $I - V$ curves from simulation and experiment. The solid circles, open squares and crosses represent the experimental data, Bohm simulation and experimentally-based mobility simulation respectively
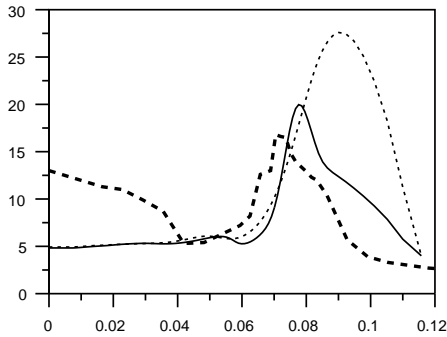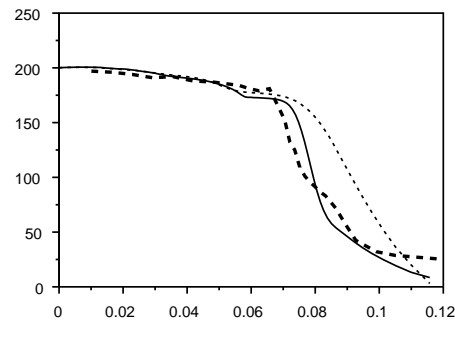

FIGURE 4. Temperature profile.

FIGURE 5. Potential profile.

potential drop takes place outside the channel in the Bohm simulation. On the contrary, experiment indicates that most of the potential drop and resulting ion acceleration happen just inside of the channel exit. The experimentally-based mobility simulation captures this quite well, as Figure 5 shows. Other plasma profiles as well as simulations using the SPT geometry (not shown) convey a similar conclusion.

The main lesson from the simulations in the $r-z$ model is that a) a simple Bohm model for the mobility is inadequate in reproducing $I - V$ curves and equilibrium profiles, and b) in the absence of sound electron transport theory-based models, experimentally-based approaches for the mobility appear rather necessary in $r - z$ codes.

3. $z - \theta$ model

3.1. Overview

While the use of an experimentally-based expression for the mobility in the $r - z$ model gave improved the results, it is still limiting for a model to depend so critically on an *ad hoc* transport parameter. Motivated by this fact, we formulate a new model for Hall

thruster plasmas. First, we construct the simplest description able to treat electron transport self-consistently. In particular, the new description must resolve the inhomogeneous Hall current and the associated azimuthal fluctuations. Azimuthal waves have been seen experimentally in a number of Hall thrusters. Their amplitude is large and their power spectrum complex, with coherent structures among random, broadband turbulence. Linear stability analysis have predicted azimuthal unstable waves at low frequency (a few hundred kilohertz) and at high frequency (megahertz), driven unstable by resistivity and equilibrium gradients in plasma density and magnetic field (Choueiri 2001). Azimuthal fluctuations in the electric potential, if properly correlated with density fluctuations, can then result in a net axial electron transport. A nonlinear theory describing this procress is presently absent, except under simplifying assumptions. An example is the theory of Yoshikawa and Rose (Yoshikawa & Rose 1962), which predicts a Bohm scaling for the electron transport with a coefficient proportional to the relative electron density fluctuation power. An objective of the model presented in this paper is to gain understanding about the azimuthal fluctuations and their associated transport.

The $z - \theta$ model draws from our experience with the $r - z$ model. It is 2D (in the axial and azimuthal directions), and hybrid in nature: the neutrals and ions are described as particles and the electrons are described as a fluid. The treatment of the ions and the neutrals follows that of the $r - z$ model. Particle injection is done by inverting a Maxwellian flux distribution function (Birdsall & Langdon 1991). The nonlinear ionization rate is given by a fit to experiment according to the following formula (Ahedo, Martinez-Cerezo & Martinez-Sanchez 2001):

$$\dot{n}_e = n_e n_n 5 \times 10^{-20} \sqrt{\frac{8T_e}{\pi m_e}} \left(1 + \frac{T_e E_i}{(T_e + E_i)^2}\right) \exp -E_i/T_e \tag{3.1}$$

The main differences in the $z - \theta$ model come from the electron fluid description. The equations governing the electron fluid are current continuity, perpendicular momentum balance, and parallel momentum balance. The system is closed with an equation for the electric field and quasineutrality. We make two assumptions: a) The magnetic field is purely in the radial direction and only a function of axial position and b) the electron temperature is only a function of axial position and it is assumed constant. The last assumption is particularly severe: we make it at this point in order to simplify the system. As we begin to get results and understand the model, a time-dependent temperature equation with all the necessary physics like ionization, joule heating, wall damping including sheath saturation effects (Barral, Makowski, Peradzynski, Gascon & Dudeck 2003), and conductive and convective fluxes will be implemented. In time, the first assumption will be relaxed as well. In fact, it has been noted that the azimuthal asymmetry in the external magnetic field arising from the magnetic configuration is associated with mode-locking (Cappelli 2004). With these assumptions the electron equations become:

$$0 = \nabla \cdot (n_e \mathbf{v_e} - n_i \mathbf{v_i}) \tag{3.2}$$

$$u_{ez} = -\mu_\perp E_z - \frac{D_\perp}{n_e} \frac{\partial n_e}{\partial z} - \frac{1}{1 + (\nu/\omega_c)^2} \frac{E_\theta}{B} - \frac{1}{1 + (\nu/\omega_c)^2} \frac{kT_e}{en_e Br} \frac{\partial n_e}{\partial \theta} \tag{3.3}$$

$$u_{e\theta} = -\mu_\perp E_\theta - \frac{D_\perp}{n_e r} \frac{\partial n_e}{\partial \theta} + \frac{1}{1 + (\nu/\omega_c)^2} \frac{E_z}{B} + \frac{1}{1 + (\nu/\omega_c)^2} \frac{kT_e}{en_e B} \frac{\partial n_e}{\partial z} \tag{3.4}$$

$$\phi = \frac{kT_e}{e} \ln n_e + \phi^* \tag{3.5}$$

$$\mathbf{E} = -\nabla\phi \tag{3.6}$$

$$n_i = n_e \tag{3.7}$$

where u_{ez} is the axial electron velocity, $u_{e\theta}$ is the azimuthal electron velocity, $\mu_\perp$ is the classical perpendicular mobility, ν is the electron-neutral collision frequency, ω_c is the electron gyro-frequency, and $D_\perp$ is the classical diffusion coefficient arising from electron-neutral collisions. The last four quantities are given by:

$$\mu_\perp = \frac{\frac{e}{m_e\nu}}{1 + (\omega_c/\nu)^2} \tag{3.8}$$

$$\nu = n_n\sigma_{en}\overline{c}_e \tag{3.9}$$

$$\omega_c = \frac{eB}{m_e} \tag{3.10}$$

$$D_\perp = \frac{\frac{kT_e}{m_e\nu}}{1 + (\omega_c/\nu)^2} \tag{3.11}$$

Finally, $\sigma_{en} = 27 \times 10^{-20} m^2$ is the approximate electron-neutral elastic collision cross section in the range of interest, $\overline{c}_e = \sqrt{\frac{8T_e}{\pi m_e}}$ is the electron thermal velocity, and m_e is the electron mass. The rest of the symbols have the same meaning as in the $r - z$ model.

We note that the axial electron velocity (eqn. 3.3) now has components proportional to E_θ and $\frac{\partial n_e}{\partial\theta}$. These terms are proportional to $\frac{1}{1+(\nu/\omega_c)^2}$, and thus they are important at low neutral densities and high magnetic fields. We expect these terms to dominate for most of the channel, but especially at the exit, where ionization depletes the neutral concentration and the magnetic field is strongest. In the opposite limit – at high neutral densities and low magnetic fields characteristic of the anode region – these terms are small. Indeed, the electron transport seen in the experiment around the anode appears to be classical. The azimuthal electron fluid velocity, $u_{e\theta}$, is given by equation 3.4. The physics associated with this equation was absent in the $r - z$ model and it is an integral part of the current model. In high magnetic field and low neutral density regions, $u_{e\theta}$ is dominated by $E \times B$ and diamagnetic drifts, the third and fourth terms of equation 3.5, respectively. As before, the electric field (eq. 3.6) is purely electrostatic and the parallel momentum equation results in a Boltzmann relation (eq. 3.5). Quasineutrality (eq. 3.7) closes the system, with n_i obtained from the ion particles via the PIC method.

The solution of the equations above yields the electric field and electron fluid velocities. Bilinear interpolation of ion particle positions gives, by quasineutrality, the plasma density. The axial electron current $n_e u_{ez}$ is then obtained as well as an effective mobility. This mobility can be compared with the "classical" value and an assessment of fluctuation-induced transport can be made.

3.2. Numerical method

The SHT geometry is used in the simulations: the axial coordinate extends from $z = 0$ to $z = .12$ (from the anode to 4 cms past the channel exit). The azimuthal coordinate is periodic. For simplicity, a uniform rectangular grid in z and θ is used with 51×50 grid points. The constant external magnetic field, assumed to be purely in the radial direction, is obtained from experiment. The electron temperature, assumed constant and only a function of axial position, is also obtained from experiment. In testing the code, uniform and gaussian profiles for the magnetic field and electron temperature are used as well.

The PIC portion of the $z - \theta$ code follows that of the $r - z$ code and has already been discussed above. We now discuss the solution of the electron fluid equations. In the present geometry, current conservation (eqn. 3.2) and quasinetrality (eqn. 3.7) can be combined to give:

$$\frac{1}{r}\frac{\partial(n_e u_{i\theta})}{\partial\theta} + \frac{\partial(n_e u_{iz})}{\partial z} - \frac{1}{r}\frac{\partial(n_e u_{e\theta})}{\partial\theta} - \frac{\partial(n_e u_{ez})}{\partial z} = 0 \tag{3.12}$$

Expressions for the azimuthal and axial components of the electric field can be obtained from equations 3.5 and 3.6 as follows:

$$E_\theta = -\frac{1}{r}\left(\frac{\partial\phi^*}{\partial\theta} + \frac{kT_e}{en_e}\frac{\partial n_e}{\partial\theta}\right) \tag{3.13}$$

$$E_z = -\frac{\partial\phi^*}{\partial z} - \frac{k\ln n_e}{e}\frac{\partial T_e}{\partial z} + \frac{kT_e}{en_e}\frac{\partial n_e}{\partial z} \tag{3.14}$$

Substituting equations 3.13 and 3.14 into 3.3 and 3.4, and substituting the resulting equations into 3.12, yields the following equation in ϕ^*:

$$a_1\frac{\partial^2\phi^*}{\partial\theta^2} + a_2\frac{\partial\phi^*}{\partial\theta} + a_3\frac{\partial^2\phi^*}{\partial z^2} + a_4\frac{\partial\phi^*}{\partial z} + a_5 = 0 \tag{3.15}$$

where the coefficients a_1, a_2, a_3, a_4 and a_5 are given by:

$$a_1 = -\frac{n_e}{r^2}\mu_\perp \tag{3.16}$$

$$a_2 = -\frac{\mu_\perp}{r^2}\frac{\partial n_e}{\partial\theta} - \frac{n_e}{rB}\frac{\partial}{\partial z}\left(\frac{1}{1 + (\nu/\omega_c)^2}\right)$$
$$-\left(\frac{1}{1 + (\nu/\omega_c)^2}\right)\left(\frac{1}{rB}\frac{\partial n_e}{\partial z} + \frac{n_e}{rB^2}\frac{\partial B}{\partial z}\right) - \frac{n_e}{r^2}\frac{\partial\mu_\perp}{\partial\theta} \tag{3.17}$$

$$a_3 = -n_e\mu_\perp \tag{3.18}$$

$$a_4 = -n_e\frac{\partial\mu_\perp}{\partial z} + \frac{1}{1 + (\nu/\omega_c)^2}\frac{1}{rB}\frac{\partial n_e}{\partial\theta} - \mu_\perp\frac{\partial n_e}{\partial z} + \frac{n_e}{rB}\frac{\partial}{\partial\theta}\left(\frac{1}{1 + (\nu/\omega_c)^2}\right) \tag{3.19}$$

$$a_5 = \frac{1 + \ln n_e}{1 + (\nu/\omega_c)^2}\frac{k}{erB}\frac{\partial T_e}{\partial z}\frac{\partial n_e}{\partial\theta} - \frac{k\ln n_e}{e}\frac{\partial T_e}{\partial z}\left(\mu_\perp\frac{\partial n_e}{\partial z} + n_e\frac{\partial\mu_\perp}{\partial z}\right)$$
$$-\frac{kn_e\mu_\perp\ln n_e}{e}\frac{\partial^2 T_e}{\partial z^2} - \frac{k\mu_\perp}{e}\frac{\partial T_e}{\partial z}\frac{\partial n_e}{\partial z} + \frac{kn_e\ln n_e}{erB}\frac{\partial T_e}{\partial z}\frac{\partial}{\partial\theta}\left(\frac{1}{1 + (\nu/\omega_c)^2}\right)$$
$$+\frac{n_e}{r}\frac{\partial u_{i\theta}}{\partial\theta} + \frac{u_{i\theta}}{r}\frac{\partial n_e}{\partial\theta} + n_e\frac{\partial u_{iz}}{\partial z} + u_{iz}\frac{\partial n_e}{\partial z} \tag{3.20}$$

Equations 3.15-3.20 above are discretized in the θ and z directions using finite differences. The boundary conditions for the electric potential in the axial coordinate are Dirichlet at the anode ($\phi_{anode} = \phi_{discharge}$), and Dirichlet at the downstream boundary ($\phi_{exit} = 0$). In the azimuthal direction the boundary condition is periodic. Upon discretization using standard central difference formulas for the derivatives, along with the boundary conditions, the resulting system becomes block-tridiagonal. The solution is found via a direct-solve method. The electric potential and electric field components then follow from equations 3.5 and 3.13-3.14. Once the electric field is obtained, the particles are advanced, neutrals are ionized via Monte Carlo, neutrals are injected at the anode according to the given mass flow rate, and new particle densities obtained with the PIC method. The electric potential is then found again and the cycle begins again.
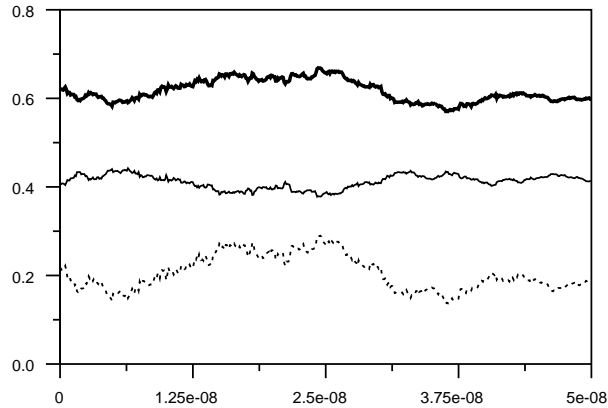
FIGURE 6. Electron current (amps) as a function of time (secs). The bold trace, solid trace and dashed trace represent the total current, the classical contribution, and the azimuthal-fluctuation induced contribution respectively.

A typical simulation is initialized with a background of ions and neutrals placed uniformly in the domain. Their velocities are obtained by inverting a Maxwellian distribution function. A key parameter in the simulation is the value of the Hall parameter, ω_c/ν. If this parameter has a small initial value (due, for instance, to a large value of n_n), the electron transport is found to be classical and azimuthal disturbances negligible. The electric field is localized axially to the region where the magnetic field is strongest and the azimuthal electric field is very small. Simulations that use uniform profiles for the magnetic field and electron temperature yield a uniform profile for the axial electric field, as expected.

However, a simulation started with a small value of the Hall parameter does not remain with that small value (except near the anode where the magnetic field is low and the neutral density is high). This is due to ionization. Ionization eventually depletes the large initial neutral density and brings up the value of the Hall parameter. Azimuthal fluctuations then emerge, along with their associated transport. Figure 6 shows the classical and anomalous contributions to electron transport, where here anomalous is taken to be the transport associated with the last two (azimuthal) terms of Equation 3.3. As shown in Figure 6, the azimuthal contributions are important. Unfortunately, numerical instability prevents us from giving further results at the present time. In fact, ionization drives strong fluctuations and eventually drives our algorithm numerically unstable.

4. Conclusions and further work

We have investigated electron transport in Hall thrusters via numerical simulation using two hybrid models, one in the radial and axial coordinates, one in the azimuthal and axial coordinates. In the $r - z$ model, the electron mobility is modeled with an *ad hoc* parameter which enhances the mobility over the classical prediction. Unlike other simulation efforts, this work uses a parameter motivated by an experimental measurement of the mobility in the Stanford Hall Thruster over a range of discharge voltages. Comparison of simulated and experimental $I - V$ curves and equilibrium profiles indicates that the experimentally-based model is superior to the simple Bohm model. This paper

concludes that, in the absence of a comprehensive nonlinear theory of electron transport, use of experimentally-based models for the mobility in $r - z$ descriptions is critical to the usefulness of such descriptions.

Motivated by the $r - z$ results, a model in the azimuthal and axial coordinates has been formulated. It represents a simplified description of Hall thruster plasmas able to capture azimuthal flows, fluctuations, and their associated transport. Preliminary results indicate that for the typical large experimental values of ω_c/ν found in these engines, the electron transport associated with azimuthal disturbances is significant. However, numerical stability has prevented us from running the model to long time scales.

Our future work with the $r - z$ model lies in a) implementing a realistic wall-damping model for the electron temperature that includes the physics of temperature-dependent secondary electron emission as well as sheath saturation effects, and b) improving the PIC portion of the code by adding more collisional effects, important for the investigation of erosion patterns in these devices. Future work with the $z - \theta$ model involves a) improving the numerical stability of the method of solution, b) examining the azimuthal fluctuations and transport in detail, and c) incorporating a temperature equation with a realistic wall-damping model.

REFERENCES

ADAMS, J. C., HERON, A. & LAVAL, G. 2004 Study of stationary plasma thrusters using two-dimensional fully kinetic simulations. *Phys. Plasmas* **11**, 295-305.

AHEDO, E., MARTINEZ-CEREZO, P. & MARTINEZ-SANCHEZ, M. 2001 One-dimensional model of the plasma flow in a Hall thruster. *Phys. Plasmas* **8**, 3058-3068.

ALLIS, M. K., GASCON, N., VIALARD-GOUDOU, C., CAPPELLI, M. A. & FERNANDEZ, E. 2004 A comparison of 2D hybrid Hall thruster model to experimental measurements AIAA-2004-3951, 40th AIAA/ASME/SAE/ASEE Joint Propulsion Conference, Ft. Lauderdale, FL.

BARRAL, S., MAKOWSKI, K., PERADZYNSKI, Z., GASCON, N. & DUDECK, M. 2003 Wall material effects in stationary plasma thrusters: near-wall and in-wall conductivity *Phys. Plasmas* **10**, 4137-4152.

BAREILLES, J., HAGELAAR, G. J. M., GARRIGUES, L., BONIFACE, C., BOEUF, J. P. & GASCON, N. 2004 Critical assessment of a two-dimensional hybrid Hall thruster model: Comparisons with experiments *Phys. Plasmas* **11**, 3035-3046.

BIRDSALL, C. K. & LANGDON, A. B. 1991 *Plasma Physics via Computer Simulation.* IOP Publishing Ltd.

CAPPELLI, M. A. 2004 *Private communication.*

CHOUEIRI, Y. E. 2001 Plasma oscillations in Hall thrusters. *Phys. Plasmas* **8**, 1411-1426.

FERNANDEZ, E., CAPPELLI, M. A. & MAHESH, K. 1998 2D simulations of of Hall thrusters. *CTR Annual Research Briefs*, 81-91.

FIFE, J. M. 1995 Two-dimensional hybrid particle-in-cell modeling of Hall thrusters. S.M. thesis, MIT.

FIFE, J. M., MARTINEZ-SANCHEZ, M. & SZABO, J. 1997 A numerical study of low-frequency discharge oscillations in Hall thrusters. AIAA-97-3052, 33rd AIAA/ASME/SAE/ASEE Joint Propulsion Conference, Seattle, WA.

GASCON, N., ALLIS, M. K., THOMAS, C. A., CAPPELLI, M. A. & FERNANDEZ, E. 2004 A closer look at longitudinal oscillations inside a Hall thruster. AIAA-2004-

3780, 40th AIAA/ASME/SAE/ASEE Joint Propulsion Conference, Ft. Lauderdale, FL.

GULCZINSKI, P. & SPORES, R. 1996 Analysis of Hall-Effect Thrusters and Ion Engines for Orbit Transfer Missions. AIAA-96-2973, 32nd AIAA/ASME/SAE/ASEE Joint Propulsion Conference, Lake Buena Vista, FL.

HIRAKAWA, M. & ARAKAWA, Y. 1996 Numerical Simulation of Plasma Particle Behavior in a Hall Thruster. AIAA 96-3195, 32nd AIAA/ASME/SAE/ASEE Joint Propulsion Conference, Lake Buena Vista, FL.

JANES, G. & LOWDER, R. 1966 Anomalous Electron Diffusion and Ion Acceleration in a Low-Density Plasma. *Phys. Fluids* **9**, 1115-1123.

LENTZ, C. A. 1990 Transient One Dimensional Numerical Simulation of Hall thrusters. S.M. thesis, MIT.

MEEZAN, N., HARGUS, W. & CAPPELLI, M. 2001 The anomalous electron mobility in a coaxial Hall discharge plasma. *Phys. Review E.* **63**, 26410-26416.

MOROZOV, A., ESINCHUK, Y., TILININ, G., TROFIMOV A., SHAROV Y. & SHCHEPKIN G. 1972 Plasma accelerator with closed electron drift and extended acceleration zone. *Sov. Phys. - Tech. Phys.* **17**, 38-45.

YOSHIKAWA, S. & ROSE, D. 1962 Anomalous diffusion of a plasma across a magnetic field. *Phys. Fluids.* **3**, 334-340.